

Supporting Information for:

North America's Midcontinent Rift Magma Volume: a coincidental rendezvous of a plume with a rift

Prasanna Mahesh Gunawardana^{1,2}, Robert Moucha², Tyrone O. Rooney³, Seth Stein⁴, and Carol A. Stein⁵

(1) now at Monash University, Earth, Atmosphere and Environment Melbourne, VIC, Australia

(2) Syracuse University, Department of Earth and Environmental Sciences, Syracuse, NY, United States

(3) Michigan State University, Department of Earth and Environmental Sciences, East Lansing, MI, United States

(4) Northwestern University, Department of Earth and Planetary Sciences, Evanston, IL, United States

(5) University of Illinois at Chicago, Earth and Environmental Sciences, Chicago, IL, United States

Methods: Governing Equations

We use a 2D thermomechanical numerical code based on the primitive variable particle-in-cell finite-difference method developed by Taras Gerya and others (Gerya, 2010; & references therein). We solve the system of equations for conservation of mass and momentum:

$$\frac{\partial v_x}{\partial x} + \frac{\partial v_y}{\partial y} = 0, \quad \frac{\partial \sigma'_{xx}}{\partial x} + \frac{\partial \sigma'_{xy}}{\partial y} - \frac{\partial P}{\partial x} = 0, \quad \frac{\partial \sigma'_{yy}}{\partial y} + \frac{\partial \sigma'_{yx}}{\partial x} - \frac{\partial P}{\partial y} = -g\rho \quad (1)$$

where g is the vertical component of the gravity; P is the pressure (mean normal stress); v_x and v_y are the horizontal and vertical components of the velocity vector v ; ρ is the density given by the equation of state;

$$\rho = \rho_r [1 + \beta(P - P_r)][1 - \alpha(T - T_r)] \quad (2)$$

in which ρ_r is the density of a material at the reference pressure P_r (10^5 Pa) and temperature T_r

(273 K); β and α are the compressibility and coefficient of thermal expansion; and σ'_{ij}

corresponds to the deviatoric stress tensor

$$\sigma'_{ij} = \sigma_{ij} + P \delta_{ij} \quad (3)$$

where σ_{ij} is hydrostatic stress. The deviatoric stress components can be formulated via the strain rate tensor components $\dot{\epsilon}_{ij}$ and effective viscosity η

$$\sigma'_{ij} = 2\eta\dot{\epsilon}_{ij}, \quad \dot{\epsilon}_{ij} = \frac{1}{2}\left(\frac{\partial v_i}{\partial x_j} + \frac{\partial v_j}{\partial x_i}\right) \quad (4)$$

The energy (heat) conservation equation in 2D is represented by the heat advection-diffusion equation;

$$\rho C_p \left(\frac{\partial T}{\partial t} + v_i \frac{\partial T}{\partial x_i} \right) = \frac{\partial}{\partial x_i} \left(k \frac{\partial T}{\partial x_i} \right) + H_r + H_s + H_a \quad (5)$$

where T is temperature, C_p is the heat capacity, H_r is the radioactive heating and k is the thermal conductivity that decreases with increasing temperature (see Supplementary Table 1). Shear heating H_s is calculated using the non-elastic strain rate and adiabatic heating H_a as:

$$H_s = \sigma_{ij} (\dot{\epsilon}_{ij} - \dot{\epsilon}_{ij}^{ela}) \quad (6)$$

$$H_a = T\alpha \frac{DP}{Dt} \quad (7)$$

We adopt a temperature-pressure dependent visco-elasto-plastic rheology based on the assumption that viscous, elastic and plastic deformations are happening under the same deviatoric stress (Gerya, 2010). The total strain rate can be represented by the summation of these three strain rate components.

$$\dot{\epsilon}_{ij} = \dot{\epsilon}_{ij}^{ela} + \dot{\epsilon}_{ij}^{vis} + \dot{\epsilon}_{ij}^{pla} \quad (8)$$

$$\dot{\epsilon}_{ij}^{ela} = \frac{1}{2\mu} \frac{D\sigma'_{ij}}{Dt}, \quad \dot{\epsilon}_{ij}^{vis} = \frac{\sigma'_{ij}}{2\eta}, \quad \text{and}$$

$$\dot{\epsilon}_{ij}^{pla} = \begin{cases} 0 & \text{for } \sigma_{II} < \sigma_{yield} \\ \frac{\chi}{2\sigma_{II}} \sigma'_{ij} & \text{for } \sigma_{II} = \sigma_{yield} \end{cases}$$

$\dot{\epsilon}_{ij}^{ela}$, $\dot{\epsilon}_{ij}^{vis}$ and $\dot{\epsilon}_{ij}^{pla}$ are elastic, viscous and plastic strain rates, respectively; $\frac{D\sigma'_{ij}}{Dt}$ is the co-

rotational objective time derivative of σ'_{ij} , μ is the shear modules; χ is the plastic multiplier and

σ_{II} is the second invariant of the stress tensor. We parametrize the plastic strength of rock, σ_{yield} , using the Drucker-Prager yield criterion in the presence of pore fluid pressure P_{fluid}

$$\sigma_{yield} = C + P \sin(\theta) \quad (9)$$

where

$$\sin(\theta) = \lambda_{fluid} \sin(\theta_{dry}), \quad \lambda_{fluid} = 1 - \frac{P_{fluid}}{P_{solid}}$$

in which the local plastic strength of rocks depends on the mean stress of the solid material $P = P_{solid}$, the cohesion C , and the effective internal friction angle θ calculated from that of dry rocks θ_{dry} , and the pore fluid pressure factor λ_{fluid} . This prescribed factor is introduced in a way that P_{fluid} reduces σ_{yield} of fractured fluid containing rock (Dymkova and Gerya, 2013; Dymkova et al., 2016). The pore fluid pressure is determined numerically with $\lambda_{fluid} = 1$ for dry rocks. Numerical models of subduction suggest $\lambda_{fluid} = 0.001$ is required for easier initiation of subduction by creating a weak layer between subducting and overriding plates (Sizova et al, 2013). In this study, we use $\lambda_{fluid} = 0.001$ that sufficiently weakens the dry continental lithosphere due to the ascending melt. Additionally, we adjust the yield criterion parameters for strain weakening using a linear model,

$$C, \sin(\theta) \begin{cases} C_0, \sin(\theta_0) & \text{for } \varepsilon \leq \gamma_0 \\ C_0 + (\varepsilon - \gamma_0) \frac{C_1 - C_0}{\gamma_1 - \gamma_0}, \sin(\theta_0) + (\varepsilon - \gamma_0) \frac{\sin(\theta_1) - \sin(\theta_0)}{\gamma_1 - \gamma_0} & \text{for } \gamma_0 < \varepsilon < \gamma_1 \\ C_1, \sin(\theta_1) & \text{for } \varepsilon \geq \gamma_1 \end{cases} \quad (10)$$

where, ε is the accumulated strain and γ_0 and γ_1 are the minimal and maximal strains, respectively.

Following, Moresi et al., (2003) and Gerya (2010), the deviatoric stress is obtained from the objective time derivative function using a backward finite-difference

$$\frac{D\sigma'_{ij}}{Dt} = \frac{\sigma'_{ij} - \sigma'^o_{ij}}{\Delta t}, \quad \sigma'_{ij} = 2\eta_{vp} \dot{\varepsilon}_{ij} Z + \sigma'^o_{ij} (1 - Z) \quad (11)$$

where

$$Z = \frac{\Delta t \mu}{\Delta t \mu + \eta_{vp}}, \quad \eta_{vp} = \begin{cases} \eta & \text{for } \sigma_{II} < \sigma_{yield} \\ \eta \frac{\sigma_{II}}{\eta \chi + \sigma_{II}} & \text{for } \sigma_{II} = \sigma_{yield} \end{cases}$$

in which Δt is the computational time-step, $\sigma_{ij}'^o$ is the deviatoric stress from the previous time step and η_{vp} is a viscosity-like Lagrangian parameter incorporating the intensity of the plastic deformation.

The effective dislocation creep viscosity is estimated as a function of both pressure and temperature of the material and is formulated in terms of stresses [Ranali,1995].

$$\eta = \frac{1}{2} A_D \sigma_{II}^{1-n} \exp\left(\frac{E_a + V_a P}{RT}\right) \quad (12)$$

where A_D is the pre-exponential factor, E_a is the activation energy, V_a is the activation volume, and n is the rheological exponent; all determined experimentally, P is the pressure, and R is the gas constant. Rock/material properties used in these simulations are listed in Supplementary Table 1.

We simulate melt production using a batch melt model in which the volumetric melt fraction M_o is assumed to increase linearly with temperature at a given pressure according to the relations below (Gerya and Yuen, 2003; Burg and Gerya, 2005).

$$M_o = \begin{cases} 0 & \text{at } T \leq T_{solidus} \\ \frac{(T - T_{solidus})}{(T_{liquidus} - T_{solidus})} & \text{at } T_{solidus} \leq T \leq T_{liquidus} \\ 1 & \text{at } T \geq T_{liquidus} \end{cases} \quad (13)$$

where

$$T_{solidus} = \begin{cases} 394 + 0.132899P - 0.000005104P^2 & \text{for } P < 10000 \text{ MPa} \\ 2212 + 0.030819(P - 10000) & \text{for } P \geq 10000 \text{ MPa} \end{cases} \quad (14)$$

$$T_{liquidus} = 2073 + 0.114P \quad (15)$$

where $T_{solidus}$ and $T_{liquidus}$ are the rock solidus and liquidus temperatures (in kelvin) as a function of pressure (in MPa) for dry asthenosphere, lithospheric mantle, and plume material (Fig. S3). We assume that melt segregates and escapes from the melting zone via channels and dykes towards the surface instantaneously in comparison to the size of the model's discrete time step [Schmeling, 2006; Gerya 2010]. However, the ascending melt weakens the rocks according to (9). At each time step, we limit the amount of melt that is transported to the surface with a melt extraction threshold $M_{max} = 4\%$ that leaves behind a non-extractable amount of melt $M_{min} = 2\%$ in the melt region [e.g. Nikolaeva et al., 2008; Sizova et al., 2010]. The total amount of melt, M , is calculated considering the previously extracted melt as follows

$$M = M_o - \sum_n M_{ext} \quad (16)$$

where $\sum_n M_{ext}$ is the amount of melt extracted during the n previous extraction events. The total amount of extracted melt during the evolution of the model is tracked by markers until 100%, at which point the marker becomes refractory. The effective density, ρ_{eff} of partially molten rock is calculated from:

$$\rho_{eff} = \rho_{solid} - M(\rho_{solid} - \rho_{molten}) \quad (17)$$

where ρ_{solid} and ρ_{molten} are densities of solid and molten rocks (*Supplementary Table 1*).

Additional References

Burg, J.-P. and Gerya, T. V. (2005) The role of viscous heating in Barrovian metamorphism of collisional orogens: thermomechanical models and application to the Lepontine Dome in the Central Alps. *Journal of Metamorphic Geology*, 23, 75–95.

Dymkova, D., Gerya, T., 2013. Porous fluid flow enables oceanic subduction initiation on earth. *Geophysical Research Letters* 40, 5671–5676.

Dymkova, D., Gerya, T., & Burg, J.-P. (2016). 2D thermomechanical modelling of continent arc–continent collision. *Gondwana Research*, 32(C), 138–150.

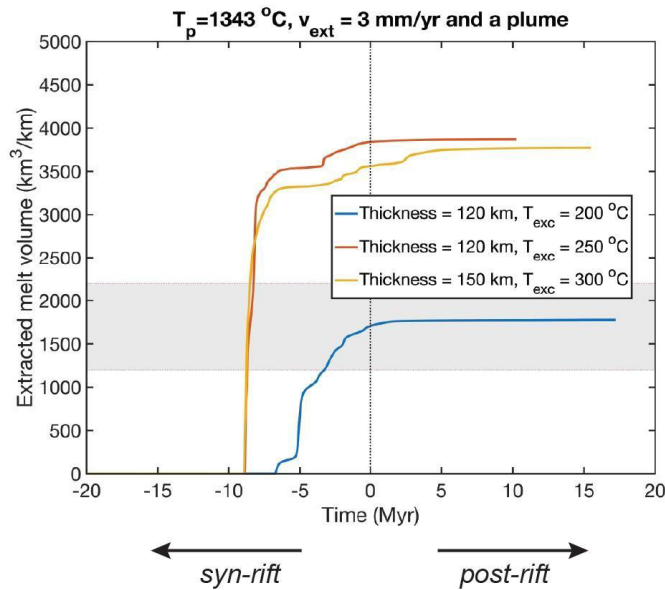
Gerya, T. V. and Yuen, D. A. (2003) Rayleigh–Taylor instabilities from hydration and melting propel cold plumes at subduction zones. *Earth and Planetary Science Letters*, 212, 47–62.

Moresi, L., Dufour, F., Mühlhaus, H.-B. (2003) A Lagrangian integration point finite element method for large deformation modeling of viscoelastic geomaterials. *Journal of Computational Physics*, 184, 476–97.

Ranalli, G. (1995) *Rheology of the Earth*. Chapman & Hall.

Sizova, E., Gerya, T., Brown, M., Perchuk, L.L., 2010. Subduction styles in the Precambrian: insight from numerical experiments. *Lithos* 116, 209–229.

a)



b)

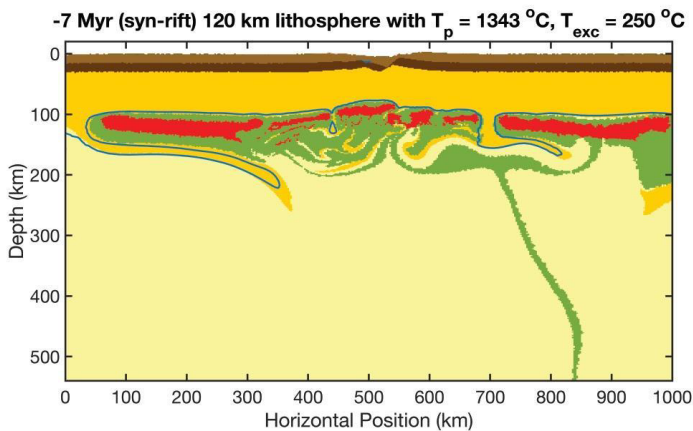


Figure S1: a) Cumulative volume of extracted melt for an extended lithosphere under present-day ambient mantle temperature T_p with a plume of temperature T_{exc} introduced during the syn-rift phase. Extension is stopped at 0 Myr once crustal thinning reaches $\beta > 3.0$. The shaded area in a) corresponds to the minimum and maximum cross-sectional area of estimated MCR flood basalt (Elling et al., 2020). The syn-rift melt volumes are extremely large as well as post-rift melt production is negligible. Therefore, this is not a viable method to simulate the MCR. b) A syn-rift snapshot of the model space, corresponding to gold line in a), depicting melt generation due to a mantle plume and lithospheric erosion by small scale convection. The 1300 °C isotherm is shown in blue.

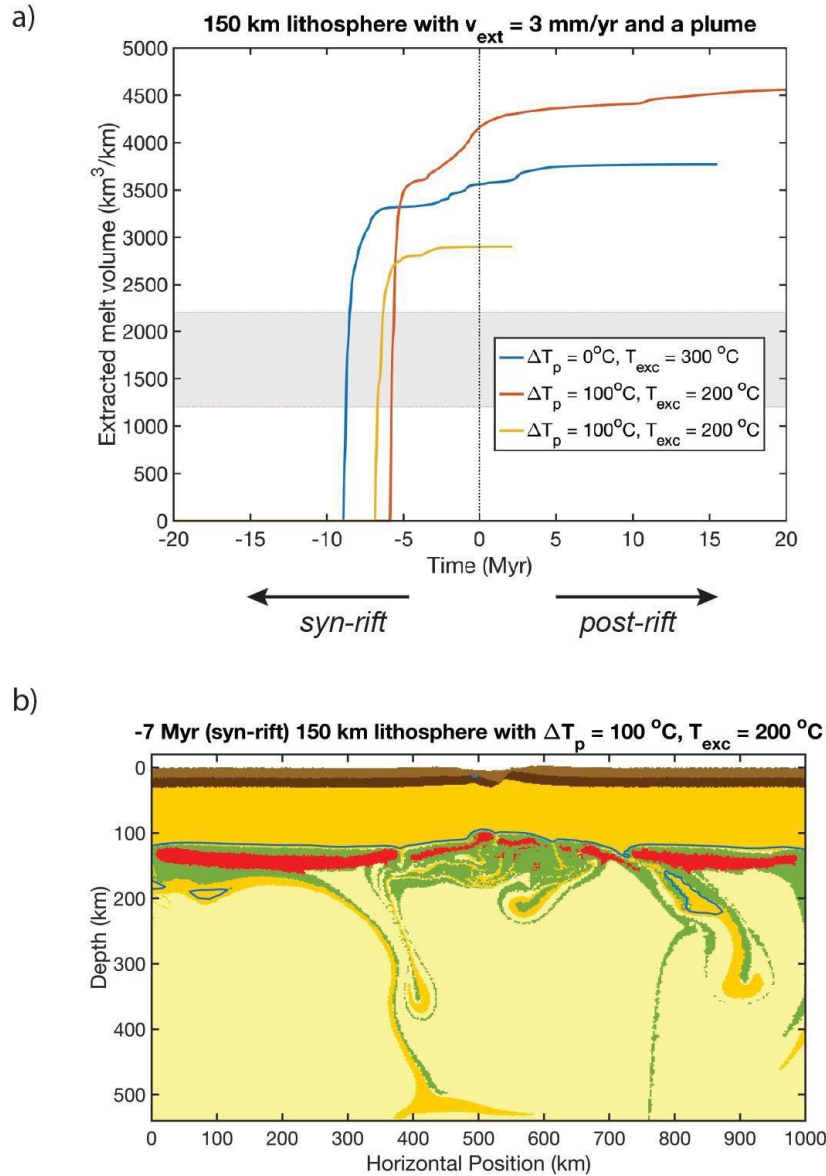


Figure S2: a) Extracted cumulative melt for an extended 150 km thick lithosphere with $\Delta T_p + T_{\text{exc}} = 300^\circ\text{C}$ as a function of time. Extension is stopped at 0 Myr once crustal thinning reaches $\beta > 3.0$. The shaded area in a) corresponds to the minimum and maximum cross-sectional area of estimated MCR flood basalt (Elling et al., 2020). The syn-rift melt volumes are extremely large, whereas the post-rift melt production is negligible. Therefore, this model is not a realistic simulation for the MCR. b) A syn-rift snapshot of the model space, corresponding to the gold line in a), depicting melt generation due to a mantle plume and lithospheric erosion by small scale convection. The 1300°C isotherm is shown in blue.

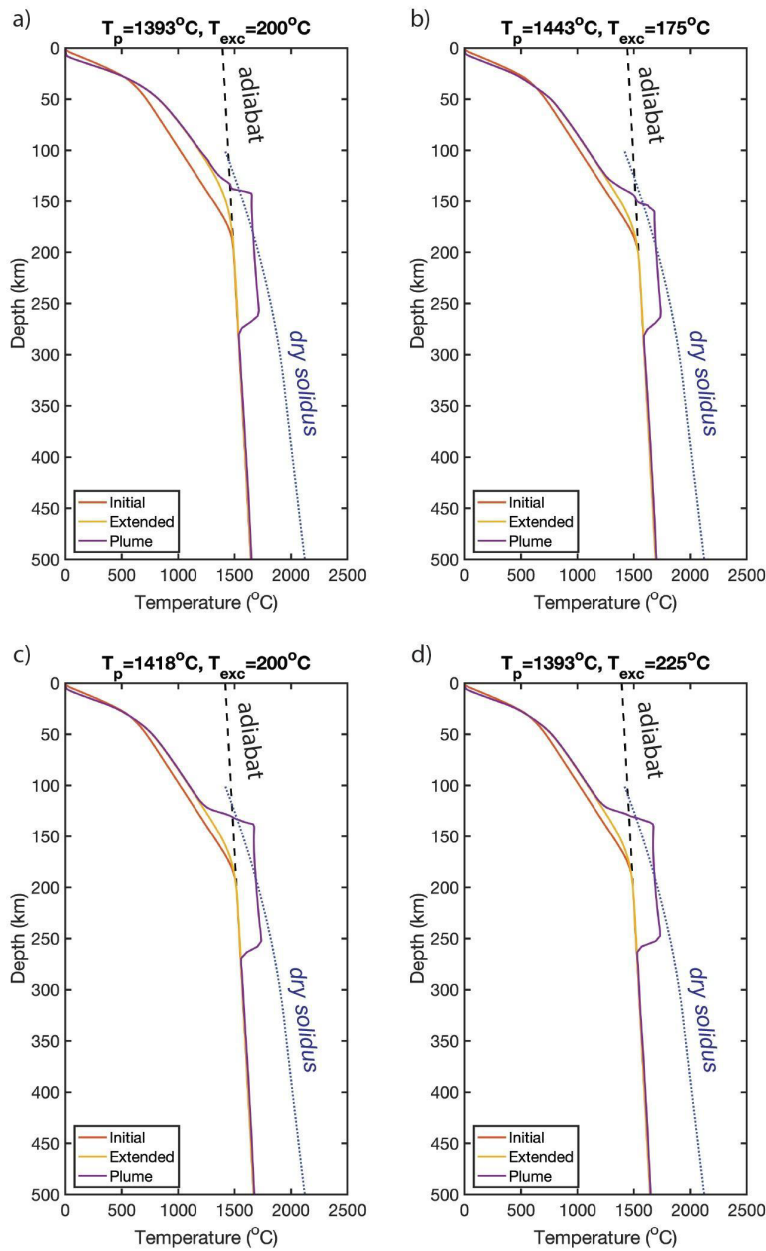


Figure S3: Geotherms corresponding to models in Figure 2c. Shown are the *initial* model geotherm, the geotherm in response to extension (*extended*) just before the arrival of the plume, and the extended geotherm perturbed by the plume head arrival (*plume*). Also shown are the adiabat intersecting the surface at corresponding mantle potential temperature T_p and the dry solidus depicting the onset of melting, Eq. 14. Panel d) corresponds to Figure 2d and simulation movie DR4 (Figure2D.mp4).

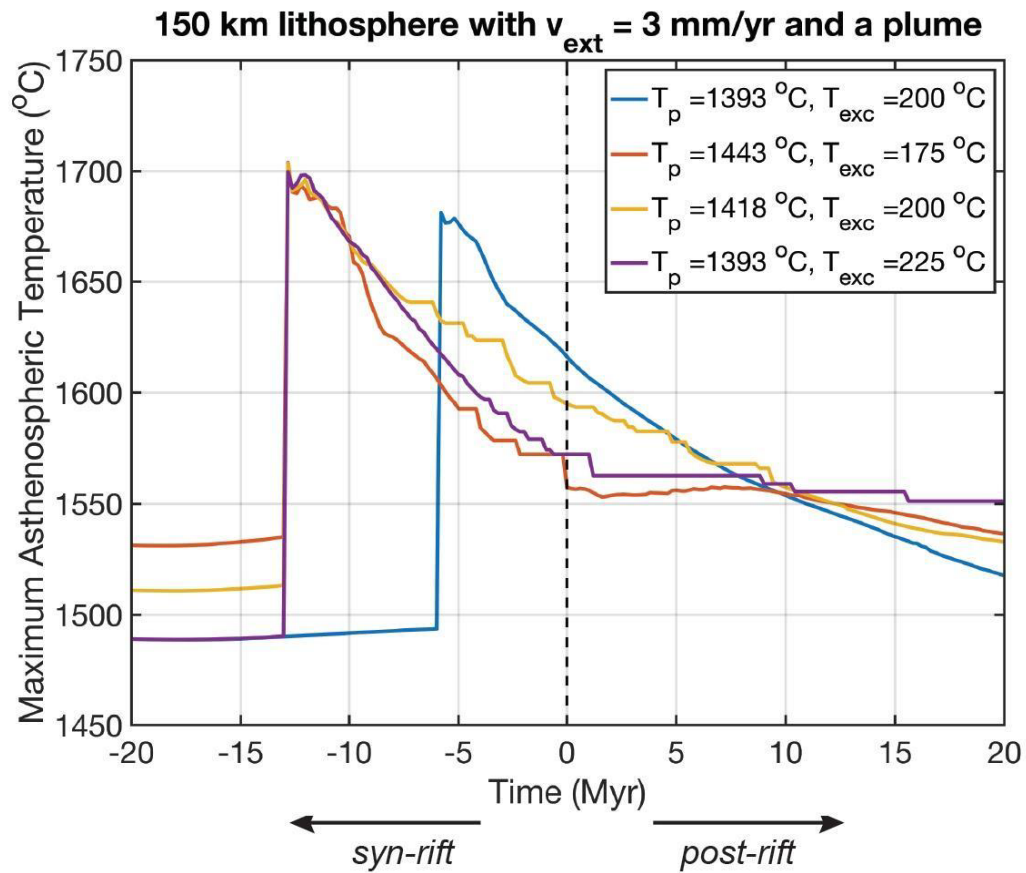


Figure S4: The maximum temperature corresponding to models in Figure 2d that is reached within the melt extraction region (Figure 1b) as a function of time relative to the end of active extension in the rift (0 Myr). The sudden increase in maximum temperature corresponds to the arrival of the plume head.

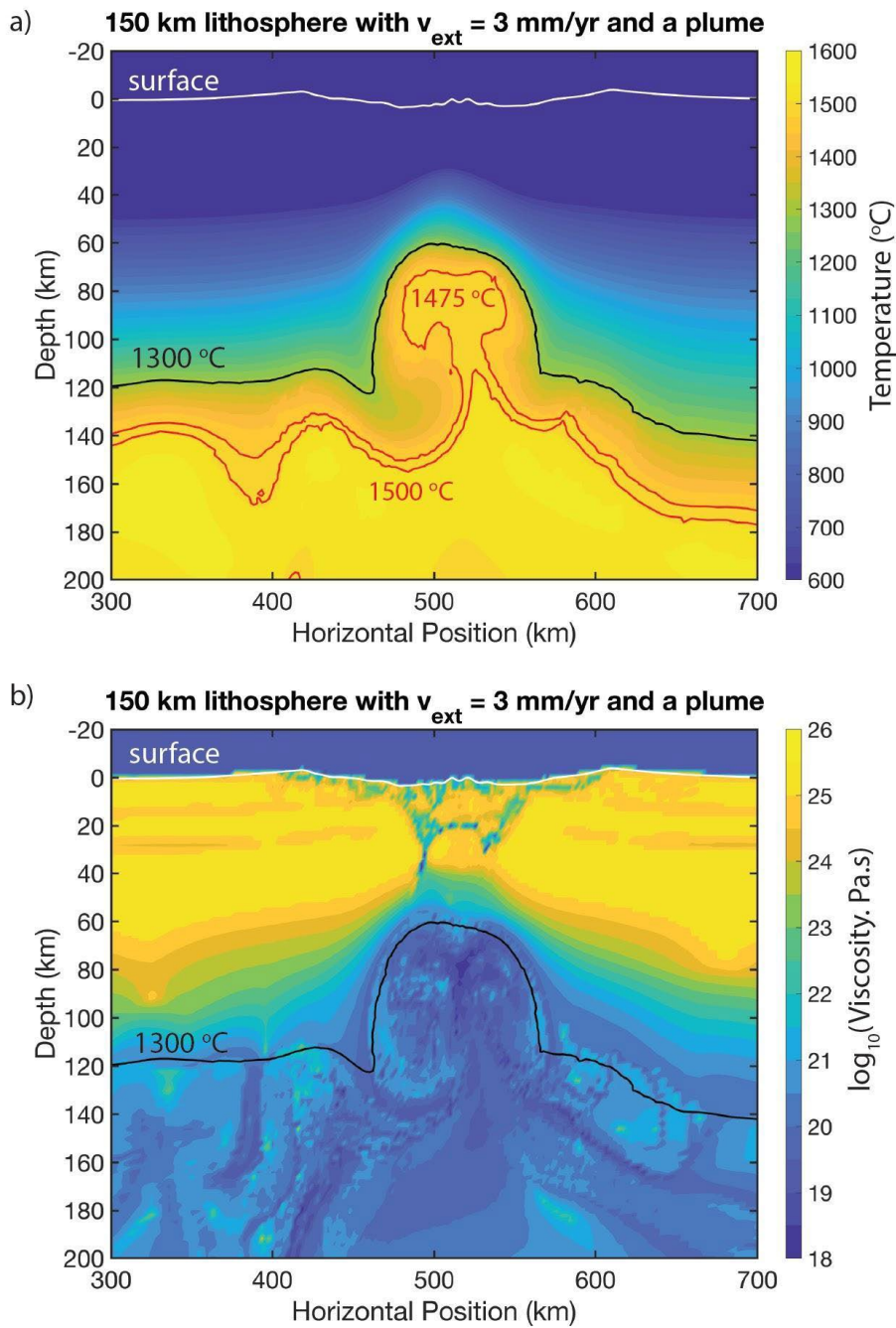


Figure S5: Temperature and viscosity distribution in a model 5.4 Myr post-rift corresponding to Figure 2d. Model mantle potential temperature $T_p = 1393$ $^{\circ}\text{C}$ and initial plume excess temperature $T_{\text{exc}} = 225$ $^{\circ}\text{C}$.

Movie Description

- 1) Supplemental Video 1 – Full simulation of manuscript Figure 2B.
- 2) Supplemental Video 2 – Full simulation of manuscript Figure 2D.
- 3) Supplemental Video 3 – Full simulation of supplementary Figure S1B.
- 4) Supplemental Video 4 – Full simulation of supplementary Figure S2B.

Symbol	Sticky air	Sediment (wet quartzite)	Upper crust (Granodiortite)	Lower crust (Diorite)	Mantle lithosphere (Dry Olivine)	Asthenosphere (Dry Olivine)	Mantle Plume (Dry Olivine)
ρ_0 (kg/m ³)	1.22	2600	2700	2850	3300	3300	3300
ρ_{melt} (kg/m ³)	-	2400	2400	2400	2900	2900	2900
α (K ⁻¹)	3×10^{-5}	3×10^{-5}	3×10^{-5}	3×10^{-5}	3×10^{-5}	3×10^{-5}	3×10^{-5}
β (Pa ⁻¹)	1×10^{-11}	1×10^{-11}	1×10^{-11}	1×10^{-11}	1×10^{-11}	1×10^{-11}	1×10^{-11}
$\Delta\rho_{\text{chem}}$ (kg/m ³)	-	0	0	0	-15	0	5
A_D (1/s/MPa ⁿ)	-	3.2×10^{-4}	3.2×10^{-4}	3.3×10^{-4}	$2.5 \times 10^{+4}$	$2.5 \times 10^{+4}$	$2.5 \times 10^{+4}$
n	-	2.3	2.3	3.2	3.5	3.5	3.5
Ea (kJ/mol)	-	154	154	238	530	530	530
Va (cm ³)	-	0	0	0	10	10	10
η (Pa.s)	$1 \times 10^{+18}$	-	-	-	-	-	-
μ (Pa)	$1 \times 10^{+20}$	$1 \times 10^{+10}$	$1 \times 10^{+10}$	$2.5 \times 10^{+10}$	$6.7 \times 10^{+10}$	$6.7 \times 10^{+10}$	$6.7 \times 10^{+10}$
C_0 (MPa)	0	10	10	10	10	10	10
C_1 (MPa)	0	3	3	3	10	10	10
$\sin(\theta_0)$	0	0	0.6	0.6	0.6	0.6	0.6
$\sin(\theta_1)$	0	0	0.075	0.075	0.6	0.6	0.3
γ_0	0	0	0	0	0	0	0
γ_1	1	1	0.1	1	1	1	1
C_p	3000	1000	1000	1000	1000	1000	1000
k_0 (W/m/K)	300	0.64	0.64	1.18	0.73	0.73	0.73
k (W/m/K)	0	$0.64 + \frac{807}{T+77}$	$0.64 + \frac{807}{T+77}$	$1.18 + \frac{474}{T+77}$	$0.73 + \frac{1293}{T+77}$	$0.73 + \frac{1293}{T+77}$	$0.73 + \frac{1293}{T+77}$
h_r (W/m ³)	0	1×10^{-6}	1.14×10^{-6}	2×10^{-7}	2.2×10^{-8}	2.2×10^{-8}	2.2×10^{-8}

Table S1. Material parameters